Unsteady Vortical Flow Around Three-Dimensional Lifting Surfaces

Mohamed Gad-el-Hak* and Chih-Ming Ho†
Flow Research Company, Kent, Washington

Flow visualization experiments were conducted in a low Reynolds number towing tank to study the time-dependent flow around two generic classes of wings. Delta and swept (including zero sweep) wings were sting mounted to a four-bar mechanism, which generated a large-amplitude, harmonic pitching motion around the one-quarter chord location at a reduced frequency that varied in the range of 0.2-3.0. Fluorescent dye layers were placed in the weakly stratified water channel prior to towing the wing. The horizontal dye sheets were excited using a vertical sheet of laser light parallel to or perpendicular to the flow direction. The dye marked the flow in the separation region around the wing, the flow in the wake region, and the potential flow away from the lifting surface. The complex, time-dependent flowfield around the different wings can be explained primarily from the mutual induction between the leading-edge separation vortex and the trailing-edge shedding vortex. The reduced frequency, the shape of the leading edge, and the wing's planform play important roles in determining the flow patterns. The effects of the finite aspect ratio on the flow around the wing are explored.

Nomenclature

AR	= aspect ratio
c	= root chord
f	= pitching frequency
K	= reduced frequency, $\pi fc/U_\infty$
R_c	= chord Reynolds number, $U_\infty c/\nu$
s	= wing semispan
t	= time, s
U_∞	= towing speed
V	= vertical velocity
V_w	= vertical velocity at the wing surface
x,y,z	= Cartesian coordinates fixed with the wing
$\alpha(t)$	= time-dependent angle of attack
ν	= kinematic viscosity

Introduction

With the recent advances in short-range infrared guided missiles, a significant change in close air combat characteristics emphasizing very fast maneuverability becomes highly desirable. This has led to a growing interest in the so-called "supermaneuverability" of fighter aircraft where previously unattained regions of the maneuver envelope are attempted, such as poststall flight maneuver and side slipping.[1,2] Current research in support of supermaneuverability involves studies to understand the dynamic stall on two- and three-dimensional lifting surfaces and the behavior of attached and separated unsteady shear layers affected by time-dependent boundary conditions, as well as attempts to exploit the unsteady flow characteristics to improve aerodynamic efficiency and enhance performance.

Aerodynamic research for time-dependent viscous flows at *high incidence* has, to date, centered primarily on the flow over two-dimensional airfoils.[3-8] The data from these studies have shed considerable light on the exceedingly complex viscous-inviscid interactions associated with time-varying flow separation. The data, furthermore, provide a meaningful base to assess numerical procedures and to develop alternative approaches as required.[9]

Two-dimensional data can play an essential role in applications having high aspect ratios (e.g., helicopter blades and commercial aircraft) where the local flow behaves, in a sense, two-dimensionally. The classic lifting line theory for an unswept wing in steady flow, for example, provides a local induced incidence correction to account for finite aspect ratio effects. This theory has been extended to include wings with sweep.[10] The lifting line concept, however, is of little value for the low-aspect-ratio wings of fighter/attack aircraft because the local airfoil section, particularly for the higher incidence angles, cannot be divorced from the wing as an entirety. Therefore, two-dimensional data play a less significant role in the design of low-aspect-ratio wings.

Considerable experimental/theoretical research has been focused on studying the flow over delta and swept wings for steady flow and time-independent boundary conditions.[11,12] Sophisticated inviscid numerical/analytical models have been developed for design purposes to describe the flowfield at high angles of attack by "modeling" the vorticity shed from the wing edges. The sharpness of the leading edge invariably fixes the location of the shed vortices feeding the leeward "conical-like" vortical motion—a factor embedded in theoretical modeling for delta wings.[13-15]

Recently, this inviscid approach has been extended to time-dependent flows by a very efficient numerical method.[16-18] The unsteadiness is an important parameter to be considered for flight maneuverability. Studies of unsteady, two-dimensional airfoils have indicated that the lift and drag experience hysteresis loops during an oscillation cycle. Corresponding information for unsteady, three-dimensional wings is very scarce.[19,20] For three-dimensional lifting surfaces, it is quite likely that inviscid techniques coupled with empiricism will be the primary short-term "engineering" tool for predicting the time-dependent flow. The long-term goal would be a Navier-Stokes solution with appropriate turbulence modeling.

The essential purpose of the present investigation was to study the time-dependent flow over three-dimensional lifting surfaces at high incidence and to provide data necessary to

Presented as Paper 85-0041 at the AIAA 23rd Aerospace Sciences Meeting, Reno, NV, Jan. 14-17, 1985; received April 2, 1985; revision received Aug. 30, 1985.

*Senior Research Scientist. Member AIAA.

†Consultant; also Professor, Department of Aerospace Engineering, University of Southern California, Los Angeles, CA. Member AIAA.

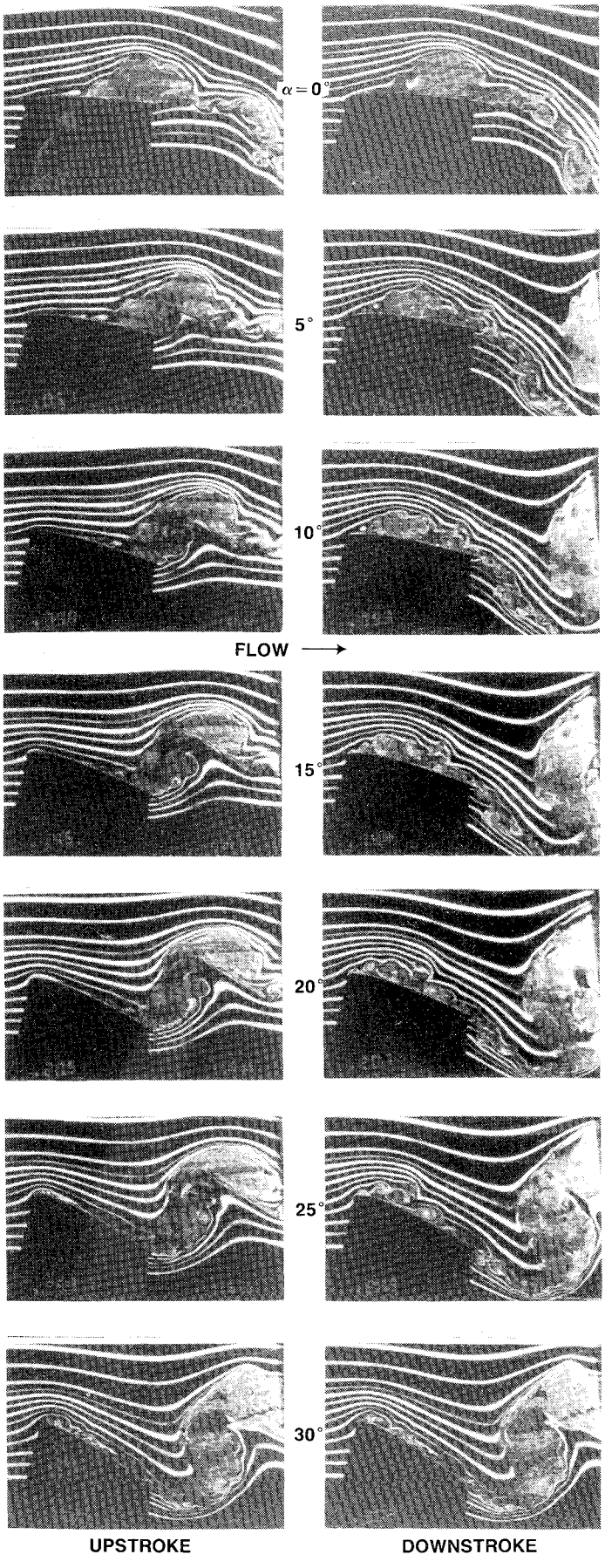

Fig. 1 Side view of NACA 0012 rectangular wing undergoing a pitching motion [$\mathcal{R}=4$, $R_c=1.25\times10^4$, $K=1.0$, $\alpha(t)^\circ=15^\circ+15^\circ\sin(1.57t)$, $z/s=0.4$].

bridge the gap from our understanding of the unsteady, two-dimensional flow about airfoils to the flow about three-dimensional wing configurations of current interest. The need to establish a detailed understanding of the physics of three-dimensional time-dependent flows coupled with the need to establish a data base to assess and to improve prediction methods provides the motivation for the present experiments. Two generic classes of wings were studied: the delta wing and the swept wing (including zero sweep). The lifting surfaces were pitched harmonically and towed in an 18 m water channel. Flow visualization techniques that utilize fluorescent dyes and sheets of laser light were used to clarify the nature of the complex flowfield around the oscillating wings. The apparatus and the visualization method are described in the next section. The effects of the operating parameters on the separation vortices are then categorized and elaborated. Conclusions are presented in the last section.

Experimental Approach

Seven lifting surfaces undergoing a harmonic pitching motion were studied. The three-dimensional surfaces were: 1) a NACA 0012 rectangular wing having a chord length of $c=12.5$ cm and an aspect ratio of $\mathcal{R}=4$; 2) a similar rectangular wing but having a flat surface and a sharp leading edge; 3) a 25 deg swept wing with a sharp leading edge, a root chord of $c=16.5$ cm, and $\mathcal{R}=4$; 4) a similar but swept forward wing; 5) a 60 deg delta wing with a sharp leading edge, $c=25$ cm, and $\mathcal{R}=2.3$; 6) a 45 deg delta wing with a sharp leading edge, $c=25$ cm, and $\mathcal{R}=4$; and 7) a similar 45 deg delta wing, but having a NACA 0012 profile at each spanwise location.

The wings were towed in the water channel described by Gad-el-Hak et al.[21] This towing tank is 18 m long, 1.2 m wide, and 0.9 m deep; the towing speed was varied in the range of 5-140 cm/s. A four-bar mechanism was used to sting mount and to pitch the wings around the desired position along the chord. In the experiments reported herein, the wings were pitched around the one-quarter chord position. The mean angle of attack could be set at 0-45 deg. A Boston Ratiotrol motor drove the four-bar linkages to produce approximately sinusoidal oscillations of amplitude ±5, ±10, or ±15 deg about a given mean angle of attack. The reduced frequency, $K\equiv\pi fc/U_\infty$ (where f is the pitching frequency and U_∞ the towing speed), was varied in the range of 0.2-3.0 and a digital readout displayed the instantaneous angle between the chord line and the towing direction $\alpha(t)$.

The complex, unsteady, separated flows around the three-dimensional lifting surfaces were visualized using the dye layer technique described by Gad-el-Hak.[22] Fluorescent dye layers were placed in the weakly stratified water channel prior to towing the wing and excited using a vertical sheet of laser light parallel to or perpendicular to the flow direction. The dye marked the flow in the separation region around the wing, the flow in the wake region, and the potential flow away from the lifting surface. The visualization results were recorded using 35 mm photographs and 16 mm ciné films (movie films are available upon request).

Results and Discussion

The seven lifting surfaces were pitched around the one-quarter chord position at a reduced requency K that varied in the range of 0.2-3.0. The wings were towed in the water channel at a root chord Reynolds number that varied in the range of 6.25×10^3 to 3.50×10^5. The dye layer technique was used to visualize the unsteady, three-dimensional flowfield around the low-pressure side of each wing.

Figure 1 is a sequence of photographs taken from the ciné film depicting a left-to-right ambient flow and the NACA 0012 rectangular wing ($c=12.5$ cm, $\mathcal{R}=4$) undergoing the pitching motion $\alpha(t)^\circ=15^\circ+15^\circ\sin(1.57t)$, where $\alpha(t)$ is the time-dependent (geometric) angle of attack and t the time in seconds. The wing was towed at a speed of $U_\infty=10$ cm/s

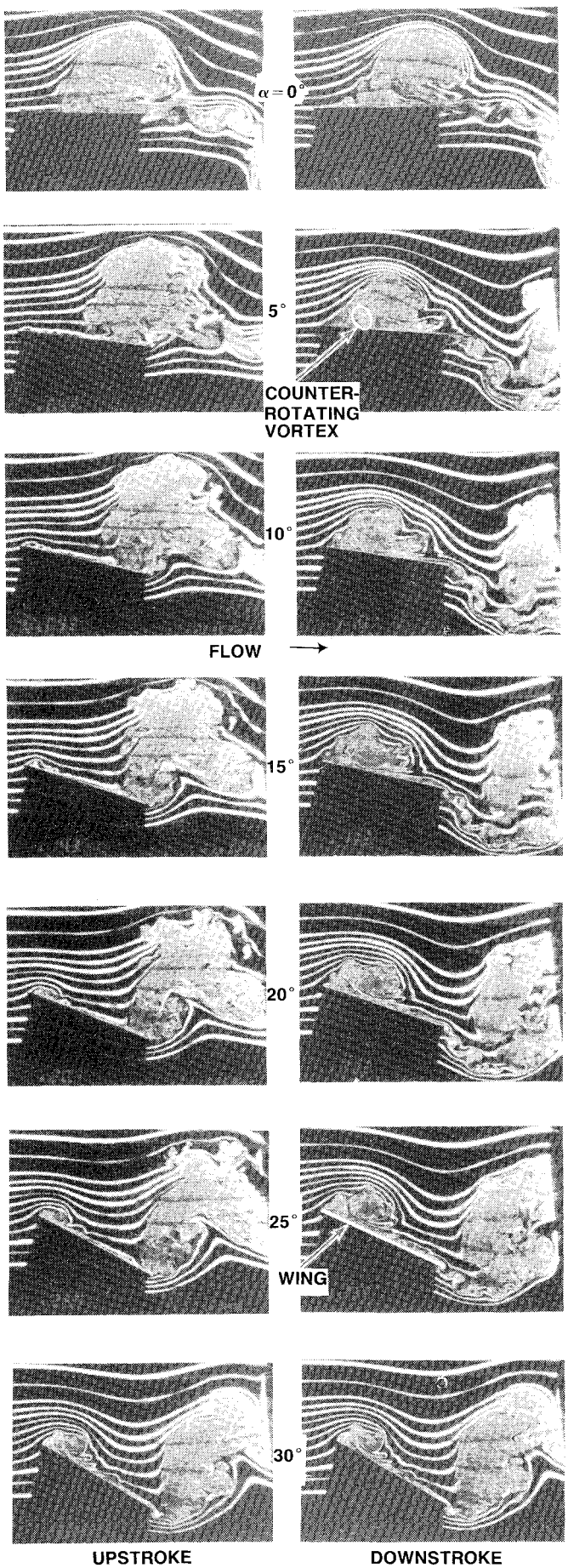

Fig. 2 Side view of sharp leading-edge rectangular wing. [$\mathcal{R} = 4$, $R_c = 1.25 \times 10^4$, $K = 1.0$, $\alpha(t)^\circ = 15^\circ + 15^\circ \sin(1.63t)$].

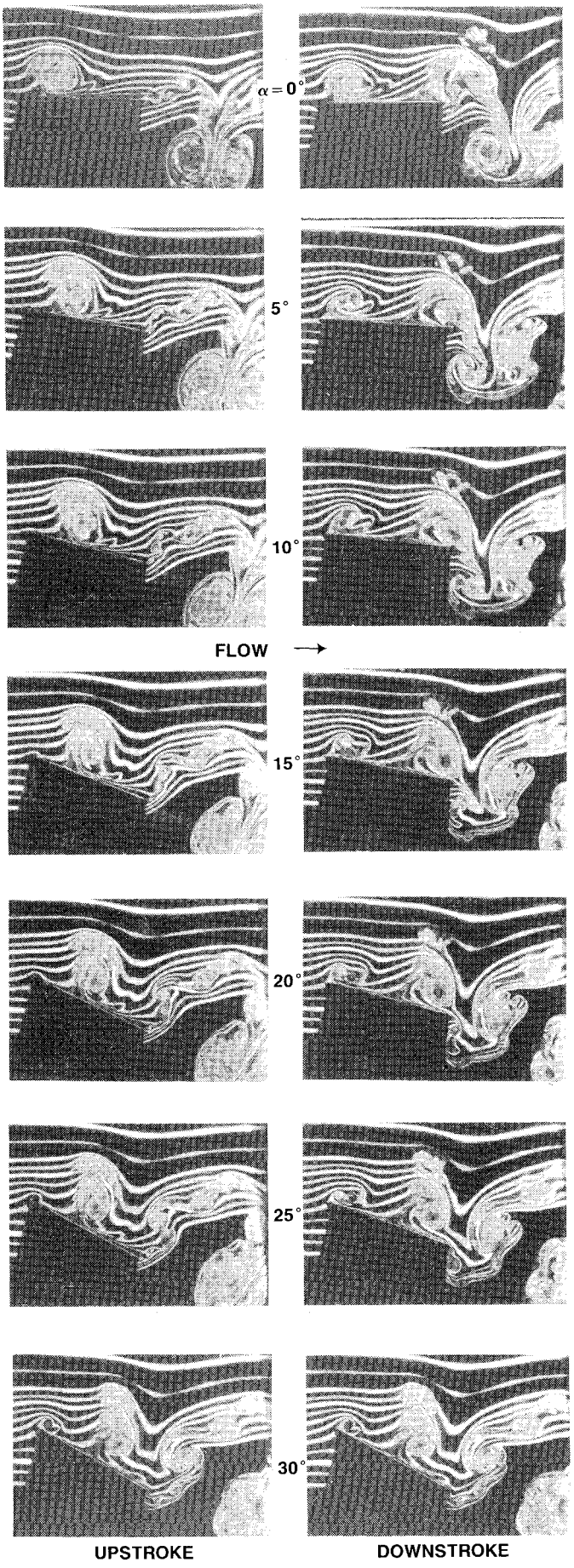

Fig. 3 Side view of sharp leading-edge rectangular wing. [$\mathcal{R} = 4$, $R_c = 8.63 \times 10^3$, $K = 3.0$, $\alpha(t)^\circ = 15^\circ + 15^\circ \sin(3.33t)$].

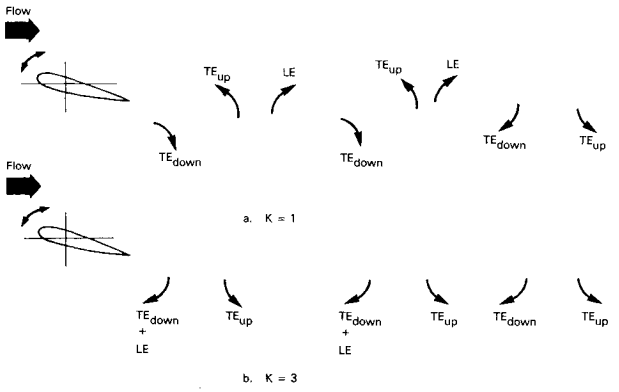

Fig. 4 Effects of reduced frequency on wake pattern behind pitching wing.

($R_c = 1.25 \times 10^4$) and the reduced frequency was $K = 1.0$. The photographs in Fig. 1 show a typical oscillation cycle‡ (0 to 30 to 0 deg) of the unsteady flowfield in a vertical plane, parallel to the flow direction and located at $z = 10$ cm (40% of the semispan s). The sheet of laser light is projected from the top of the tank and the dark area below the wing is the shadow of the lifting surface. Both the upward and downward motions of the wing are shown side by side for $\alpha = 0$, 5, 10, 15, 20, 25, and 30 deg.

The complex, unsteady flowfield associated with the pitching wing can be explained primarily from the *mutual induction* between the leading-edge separation vortex and the trailing-edge shedding vortex. At large angles of attack, the flow separates at the leading edge and a clockwise vortex is formed and convected downstream. This vortex is eventually shed from the trailing edge. When the wing is in the upstroke, the trailing edge moves downward and a shear layer is created at the upper surface. The shear layer rolls up into a counterclockwise vortex that is also shed from the trailing edge. Conversely, a clockwise vortex is formed during the downstroke. These vortices enter the wake at different phases of the cycle and result in a particular wake pattern for a given reduced frequency. For the rectangular wing pitching at the reduced frequency of $K = 1.0$, the clockwise separation vortex from the leading edge convects downstream and is shed from the trailing edge just before the wing starts the upstroke of the new cycle. During this upstroke, a counterclockwise vortex is generated at the trailing edge and forms a vortex pair with the leading-edge vortex. This vortex pair tends to convect downstream and upward, so that the induced flow above the chord is more or less cancelled. During the downstroke, a clockwise vortex is generated at the trailing edge and its induced velocity tends to thicken the separation zone above the wing.

Effects of Leading Edge Shape

Two rectangular wings having the same chord ($c = 12.5$ cm) and aspect ratio ($\mathcal{R} = 4$) were tested to determine the effects of the leading-edge shape. The first wing had a NACA 0012 cross section, while the second wing had a flat surface and a sharp leading edge. The two wings were towed at a speed of $U_\infty = 10$ cm/s ($R_c = 1.25 \times 10^4$) and were harmonically pitched around the one-quarter chord point such that $\alpha(t)^\circ = 15^\circ + 15^\circ \sin(1.6\,t)$ and $K = 1.0$. Typical oscillation cycles of the unsteady flowfield in a vertical plane, parallel to the flow direction and located at $z = 10$ cm, are shown in Figs. 1 and 2 for the blunt and the sharp leading-edge wings, respectively.

The distinct characteristic of the sharp leading-edge wing is the existence of a counter-rotating vortex upstream of the leading-edge separation vortex. Although this is more clearly indicated in the ciné film from which Fig. 2 was drawn, the outer boundaries of the counter-rotating vortex are outlined by the white circle in the still frame taken at $\alpha = 5$ deg during the downstroke. The mutual induction of the vortex pair lifts itself away from the wall and results in a large intrusion into the inviscid region. The counter-rotating vortex is not observed on the blunt leading-edge wing. In this case, the leading-edge separation vortex rolls along the chord. The separation region is much thinner than that on the sharp leading-edge wing.

The counter-rotating vortex may have important implications in controlling the unsteady flow. In the boundary layer produced by an impinging jet, a counter-rotating vortex occurs as a result of the unsteady separation produced by the shear layer vortex in the jet.[23] Large suction is generated on the impinging plate by the counter-rotating vortex. It has been speculated that the high-level, unsteady lift of pitching wings is caused by a corresponding large suction associated with a counter-rotating vortex.[24] Such a vortex has been clearly identified on the sharp leading-edge rectangular wing depicted on Fig. 2. The large suction associated with the counter-rotating vortex implies that the aerodynamic characteristics could be significantly altered by modifying the evolution of this vortex, offering the potential for enhancing the performance of a given lifting surface.

Effects of Reduced Frequency

To investigate the effects of reduced frequency on the flowfield, the sharp leading-edge rectangular wing was pitched at a frequency that varied in the range of $K = 0.2$-3.0. The root chord Reynolds number for all runs was approximately $R_c = 10^4$ and the angle of attack was $\alpha(t)^\circ = 15 \pm 15$ deg. Figures 2 and 3 show a sequence of photographs during a typical cycle at the reduced frequencies $K = 1.0$ and 3.0, respectively. The vertical laser light was parallel to the flow and was at a distance of 10 cm off the wing centerline in both cases. The difference between the $K = 1.0$ case and the $K = 3.0$ case is due to the vortex pattern in the wake. For $K = 1.0$ (Fig. 2), the clockwise leading-edge separation vortex convects downstream at about 45% of the towing speed and is shed from the trailing edge just before the wing starts the upstroke of the new cycle. During this upstroke, a counterclockwise vortex is generated at the trailing edge and forms a vortex pair with the leading-edge vortex. This vortex pair tends to convect downstream and upward, so that the induced flow above the chord is more or less cancelled. During the downstroke, a clockwise vortex is generated at the trailing edge and its induced velocity tends to thicken the separation zone above the wing.

The situation is different at $K = 3.0$ (Fig. 3). The vortex from the leading edge is convected at a slower rate relative to the oscillation period and is shed at the downstroke of the next cycle with the clockwise trailing-edge vortex. The combined vortex forms a vortex pair with the counterclockwise vortex produced in the previous upstroke. During the new upstroke, another counterclockwise vortex forms at the trailing edge and has a net effect of suppressing the thickness of the separation zone above the wing.

The wake pattern for $K = 1.0$ and 3.0 is shown schematically in Fig. 4. In this figure, TE_{up} refers to the counterclockwise vortex shed from the trailing edge during the upstroke (0-30 deg), TE_{down} refers to the clockwise vortex shed from the trailing edge during the downstroke (30-0 deg), and LE refers to the leading-edge separation vortex.

At the lowest reduced frequency ($K = 0.2$), the oscillation period is relatively long and the flow has more time to adjust to angle-of-attack variations. The trailing-edge vortices are located inside the separation zone originating form the leading edge.[22,25] The mutual induction between the two vortical zones is less clear compared to higher reduced-frequency runs. However, the general concept should still hold.

‡The first oscillation cycle is different from the second or subsequent cycles, hence the first cycle is not used in any of the figures presented here.

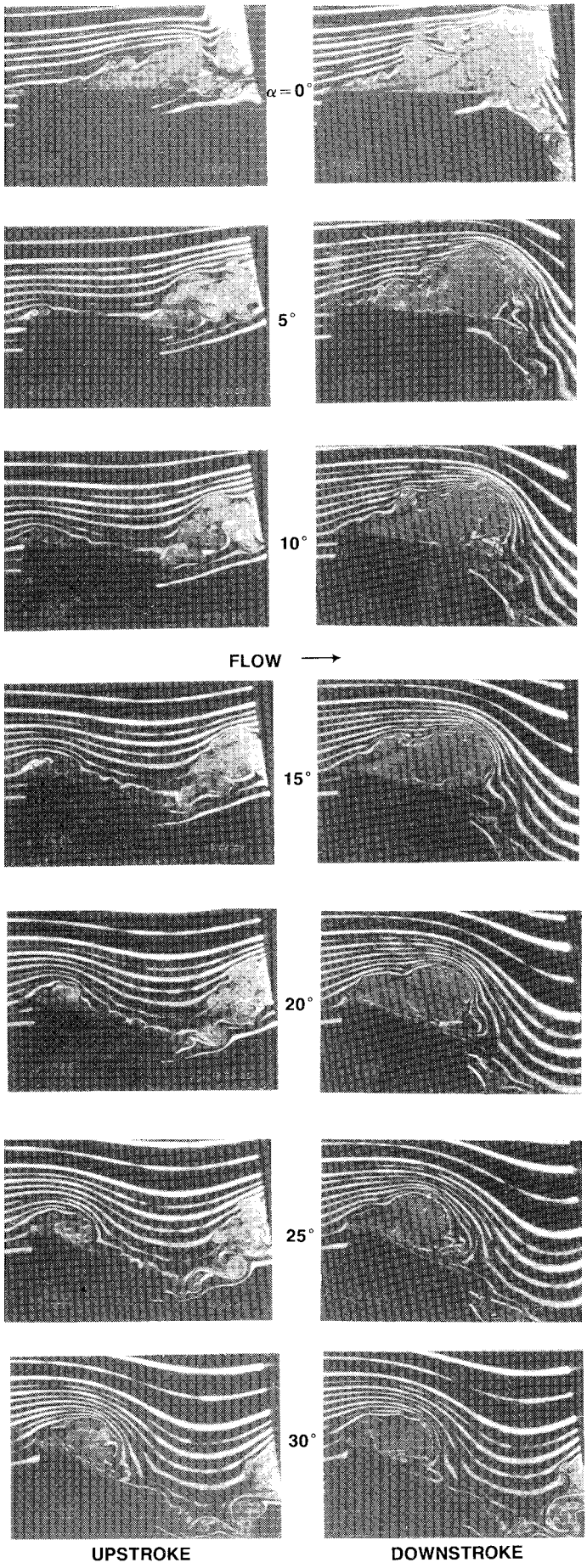

Fig. 5 Side view of sharp leading-edge swept wing. [$\mathcal{R}=4$, $R_c=1.65\times10^4$, $K=1.0$, $\alpha(t)^\circ=15^\circ+15^\circ\sin(1.19t)$].

Effects of Wing Planform

Four sharp leading-edge wings having an aspect ratio of $\mathcal{R}=4$ were tested to determine the effects of wing planform. A rectangular wing, a 25 deg swept wing, a forward swept wing, and a 45 deg swept delta wing were pitched at an angle of attack of $\alpha=15\pm15$ deg and a reduced frequency of $K=1.0$. A typical oscillation cycle of the unsteady flowfield in a vertical plane, parallel to the flow direction and located at $z=10$ cm, is shown in Figs. 2 and 5-7 for the rectangular, swept, forward swept, and delta wings, respectively.

On the rectangular wing, the leading-edge separation vortex convects downstream (Fig. 2), while it is stationary during part of the cycle on the swept wing (Fig. 5). In the ciné film from which the still photographs were drawn, a counter-rotating vortex can be seen near the leading-edge separation vortex on the forward swept wing (Fig. 6), but not on the (backward) swept wing at the present visualization station ($z=40\%$ of the semispan). This is not surprising, since the separation patterns along the span are known to be very different on backward and forward swept wings in steady flight.

On the delta wing, the leading-edge separation vortex does not convect, rather it experiences a growth-decay cycle (Fig. 7). There exists a blob of dye that moves along the chord, while the leading-edge vortex shrinks to minimum size. This blob of dye could be related to the possible separation bubble in the center part of the span.[26,27]

At one chordwise position on a delta wing ($0.8c$ from the apex), Gad-el-Hak and Ho[27] found that the vertical velocity near the center span is caused primarily by the vertical motion of the wing. In the present investigation, we further confirmed this finding by measuring, from the visualization movies, the vertical velocity V about one-quarter chord above the 60 deg sweep, sharp leading-edge delta wing along several chordwise locations. The normalized values of the vertical displacement (V/V_w) at different attack angles and at several locations along the chord were found to be constant within the experimental error.[25] This supports the hypothesis advanced by Gad-el-Hak and Ho[27] that the vertical velocity away from the wing is produced primarily by the normal motion of the wing (potential effect).

Effects of Finite Aspect Ratio

Due to the finite aspect ratio, a spanwise flow is necessary to accommodate the discontinuity at the wing tips. In the case of the pitching delta wing, a pair of vortices develops near the leading edge and experiences a growth-decay cycle with hysteresis during a pitching period.[26,27] For the rectangular wing, a streamwise vortex is formed at the tip, while a spanwise, convective vortex is generated in the center portion of the span.[19,20]

The sharp leading-edge rectangular wing was used to examine the nature of the three-dimensional flow. End views at different streamwise stations as well as side views at different spanwise locations were visualized using the dye layer technique. Figure 8 is a sequence of photographs of the pitching, sharp leading-edge rectangular wing taken with an underwater movie camera. The vertical sheet of laser was perpendicular to the flow and located at $x/c=0.8$. The wing was towed at a speed of $U_\infty=10$ cm/s ($R_c=1.25\times10^4$) and underwent the pitching motion $\alpha(t)^\circ=15^\circ+15^\circ\sin(1.6t)$ at the reduced frequency $K=1.0$. The typical oscillation cycle (0 to 30 to 0 deg) shown in Fig. 8 depicts the left side of the symmetric wing and a flow out of the plane of the photographs. Both the upward and downward motions of the wing are shown side by side for $\alpha=0$, 5, 10, 15, 20, 25, and 30 deg. The end views confirm the general model proposed by Adler and Luttges.[20] The flow could be divided into three distinct regions: the tip vortex, the leading-edge vortex, and an interaction zone.

The streamwise tip vortex undergoes a growth-decay cycle, much the same as the leading-edge vortices on a pitching delta wing.[27] The tip vortices grow during the upstroke, presumably resulting in a corresponding lift increase. The maximum size

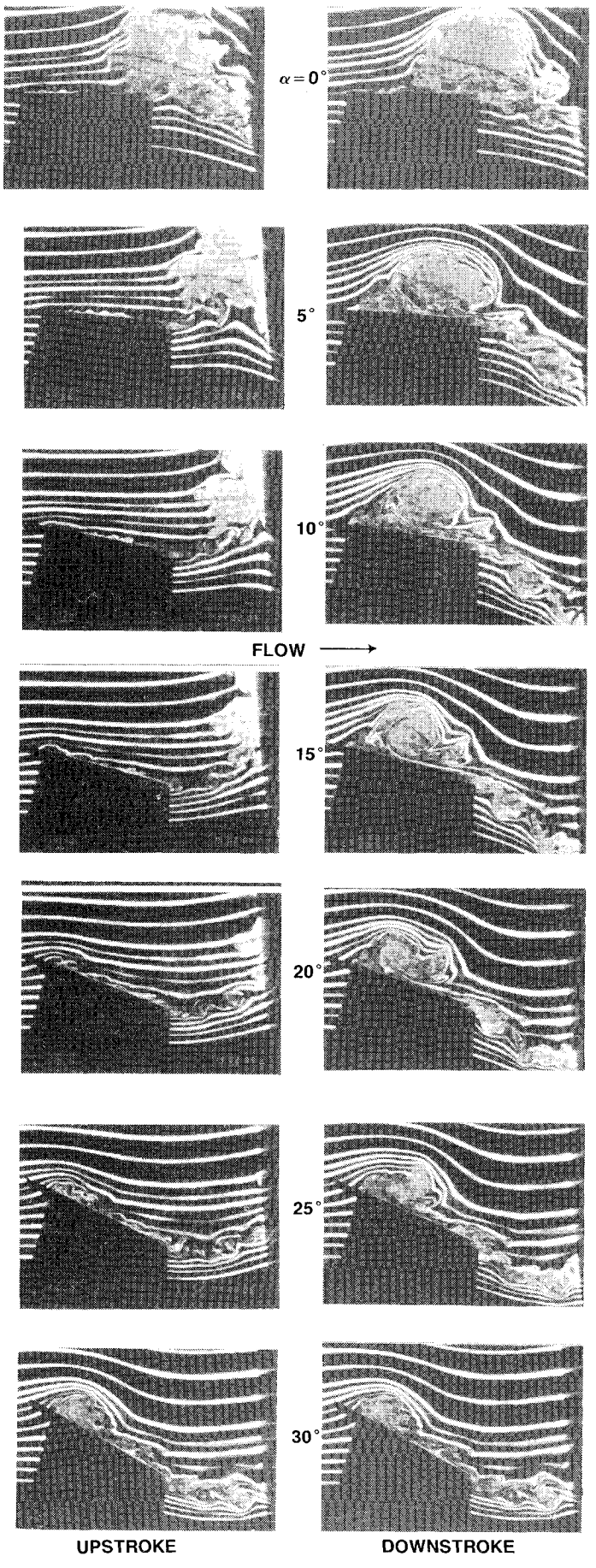

Fig. 6 Side view of forward swept wing [$\mathcal{R}=4$, $R_c=1.65\times10^4$, $K=1.0$, $\alpha(t)^\circ=15^\circ+15^\circ\sin(1.19t)$].

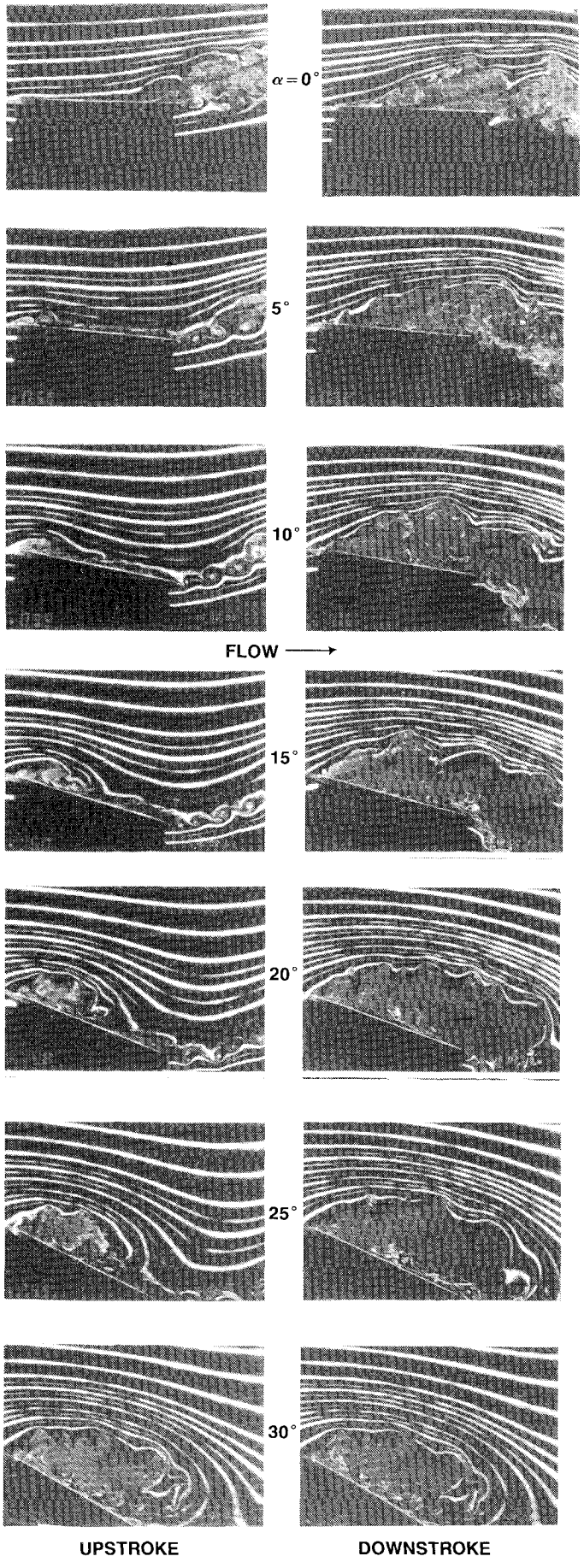

Fig. 7 Side view of 45 deg sweep, sharp leading-edge delta wing. [$\mathcal{R}=4$, $R_c=2.5\times10^4$, $K=1.0$, $\alpha(t)^\circ=15^\circ+15^\circ\sin(0.82t)$].

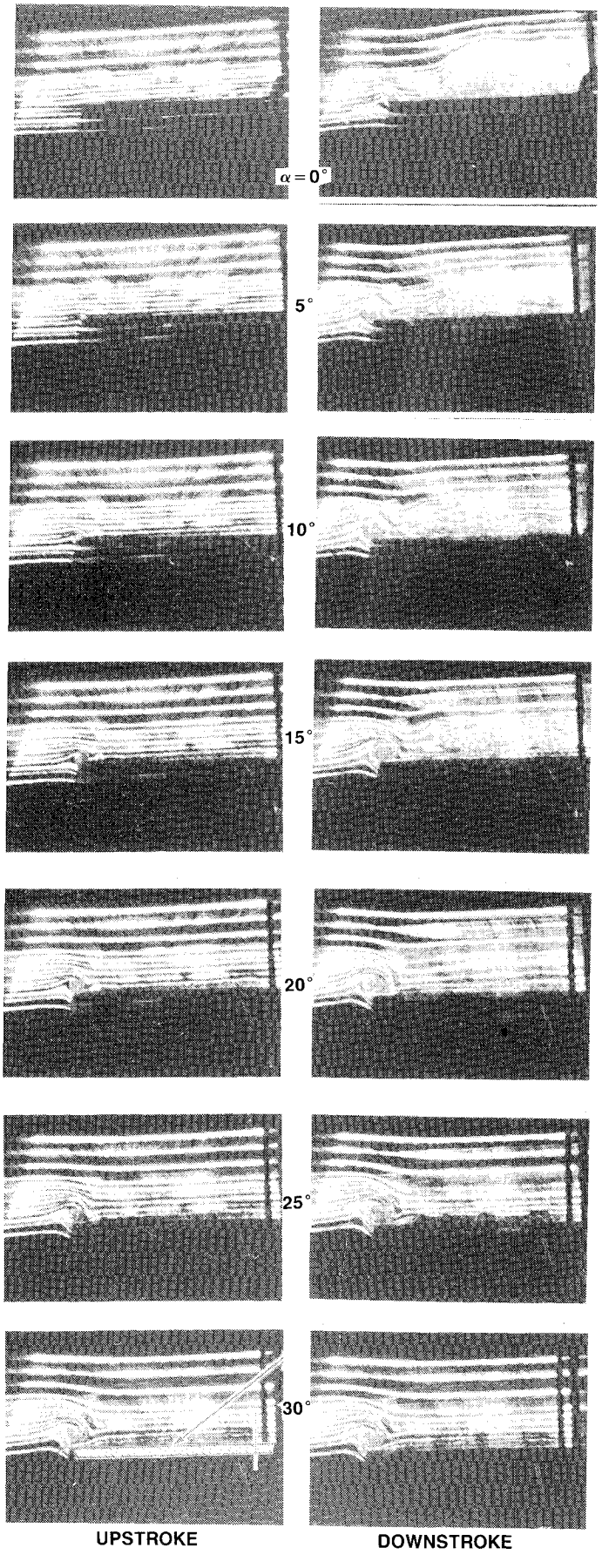

Fig. 8 End view of sharp leading-edge rectangular wing at $x/c = 0.8$ [$\mathcal{R} = 4$, $R_c = 1.25 \times 10^4$, $K = 1.0$, $\alpha(t)^\circ = 15^\circ + 15^\circ \sin(1.6t)$, flow out of plane of paper].

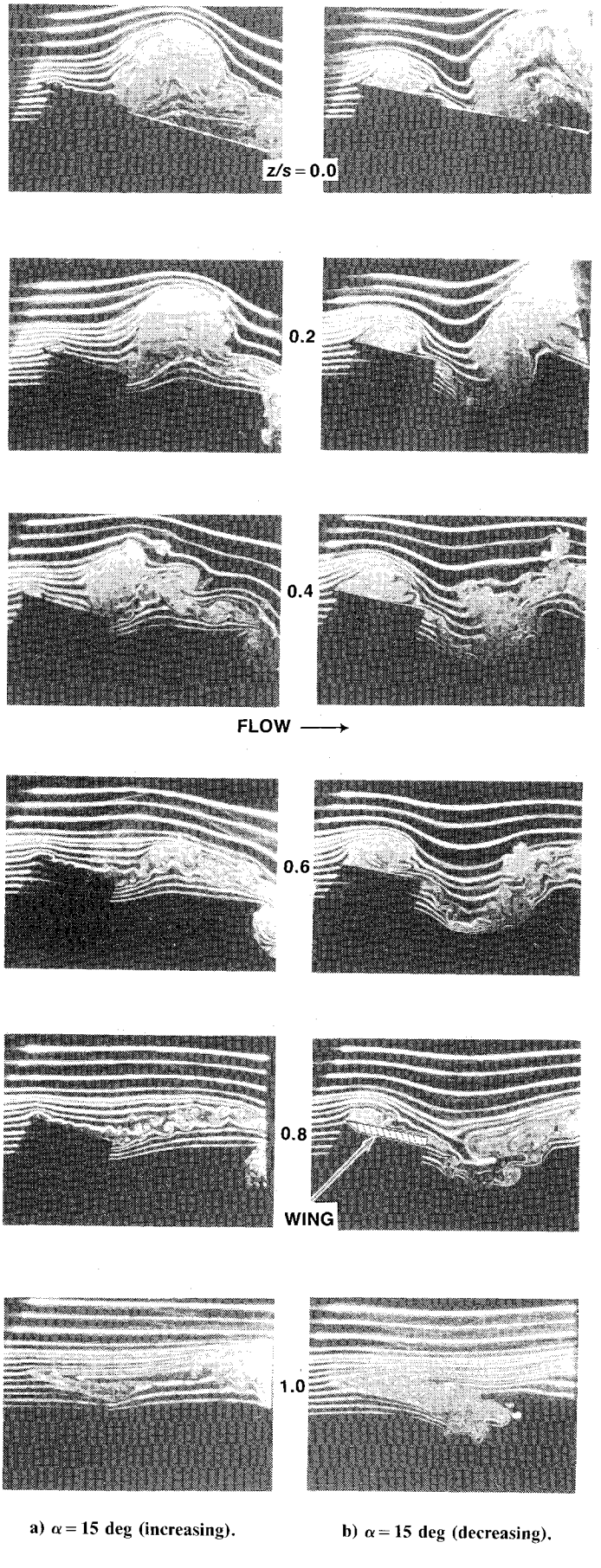

a) $\alpha = 15$ deg (increasing). b) $\alpha = 15$ deg (decreasing).

Fig. 9 Spanwise variations of the flow around sharp leading-edge rectangular wing. [$z/s = 0$, 0.2, 0.4, 0.6, 0.8, and 1.0; $K = 1.0$; $\alpha(t)^\circ = 15^\circ + 15^\circ \sin(1.6t)$].

of the tip vortex is about $0.35c$ and is reached shortly after the end of the upstroke. When the angle of attack decreases, a pair of counter-rotating vortices is generated. The emergence of the coherent, reversed vortices leads to the decay of the unsteady tip vortex.

The spanwise leading-edge vortex convects downstream, arriving at the observation station during the downstroke. It achieves its maximum height of about $0.8c$ at the completion of the oscillation cycle ($\alpha = 0$ deg) and occupies about 65% of the wing's span. This leading-edge vortex is a result of flow separation at high attack angles and is very similar to that observed on two-dimensional airfoils undergoing large-amplitude pitching motions.[3-8]

The interactive interface, identified by Adler and Luttges[20] on a pitching, finite aspect ratio wing having a NACA 0015 cross section, is located between the tip vortex and the leading edge vortex and occupies a spanwise region of about 8% of the wing's span.

The unsteady separation process on the sharp leading-edge rectangular wing can be reconstructed from side views at different spanwise locations. Figure 9 depicts events at two instances, one during the upstroke at $\alpha = 15$ deg and the second at the same angle of attack during the downstroke. The stations shown in the figure are $z/s = 0$, 0.2, 0.4, 0.6, 0.8 and 1.0, where z is the spanwise coordinate measured from the wing's centerline and s the semispan (25 cm). The run conditions are the same as those for the case shown in Fig. 8. During the upstroke (Fig. 9a) and away from the wing tip, a spanwise vortex is formed near the leding edge, while the corresponding vortex from the preceding cycle has convected into the wake of the wing. The drastic change in size of the latter vortex as the observation station is moved from the root region toward the wing tip is a dramatic demonstration of the degree of three-dimensionality of the unsteady flow. It is clear that any attempt to model such flow using a two-dimensional approximation is bound to fail. Similar strong three-dimensional effects have been observed by Winkelmann and Barlow[28] in the case of a steady flow around a low-aspect-ratio rectangular wing beyond stall.

By observing the movie sequences from which Fig. 9 was drawn, a more complete picture of the unsteady separation can be reconstructed. At the wing tip ($z/s = 1.0$), the flow separates first at $\alpha \simeq 5$ deg during the upstroke. The separation rolls up in a tip vortex and propagates upstream, eventually reaching the leading edge at $\alpha = 10$ deg. The tip vortex grows in size as the angle of attack increases and its strength is reduced when the counter-rotating vortex is produced during the downstroke. Near the root of the wing, the flow separates at the leading edge at $\alpha = 10$ deg during the upstroke. This separation seems to be evoked by the upstream-propagating separation at the wing tip. The leading-edge vortex grows in size and its convection speed varies with the oscillation phase. When the leading-edge vortex reaches the trailing edge of the wing, its vertical extent is about $0.6c$ at $z/s = 0$, and about $0.8c$ at $z/s = 0.5$. The separation vortex is not observed at the trailing edge in the interactive region ($z/s = 0.65$-0.82). Since a vortex cannot end in free space, a three-dimensional vortical structure must exist in this region.

Conclusions

The unsteady separated flow around three-dimensional lifting surfaces is dominated by large-scale vortices, about a chord length in size. Several features observed at different operating parameter ranges can be understood through the mutual induction among the leading-edge separation vortex and the vortices shed as a result of the vertical motion of the trailing edge.

The wake pattern of the rectangular wing varies significantly with the reduced frequency and is deterimined by the phase angle of the leading-edge vortex's arrival at the trailing edge. At $K = 1.0$, the wake consists of a vortex pair above the chord line and a single clockwise vortex below the chord line. The clockwise vortex induces an upward motion that results in a thick separation zone on the chord. At $K = 3.0$, the wake has a vortex pair below the chord line. The induction of the counterclockwise trailing-edge vortex suppresses the upward motion of the leading-edge vortex; hence, the separation zone on the chord is much thinner than that at $K = 1.0$.

A secondary counter-rotating vortex is clearly identified on the sharp leading-edge rectangular wing. The mutual induction between the vortex pair lifts the vortices from the wall and results in a large intrusion into the inviscid region. The separation zone is about twice as thick as that on the blunt leading-edge wing. We speculate that the counter-rotating vortex could have an important role in the generation of unsteady lift.

On the rectangular wing, the leading-edge separation vortex convects downstream, while it is stationary during part of the cycle on the swept wing. On the delta wing, the leading-edge vortex does not convect, rather it experiences a growth-decay cycle.

Additional end and side views of the sharp leading-edge rectangular wing revealed the existence of three distinct regions similar to those observed by Adler and Luttges[20] on a NACA 0015 wing: the tip vortex, which undergoes a growth-decay cycle; the leading-edge separation vortex, which convects downstream and seems to be triggered by the upstream-propagating separation near the wing tip; and the intermediate zone, where the tip vortex and the leading-edge vortex interact. The strong three-dimensional effects demonstrated in the present results make it clear that any attempt to model the unsteady flow around finite-aspect-ratio wings using a two-dimensional approximation is bound to fail.

More visualization experiments are needed to further clarify the topology of the complex vortical structures on the different wing planforms used in the present investigation. The results should then be used to design fast-response probe experiments to measure the velocity field and to correlate the visualization events with the forces and moments experienced by the pitching wing.

Acknowledgment

This work is supported by the U.S. Air Force Office of Scientific Research under Contract F49620-82-C-0020, and monitored by Maj. M. S. Francis and Dr. J. D. Wilson. The authors would like to acknowledge the valuable help of Messrs. Morton Cooper and Randy Srnsky.

References

[1]Herbst, W. B., "Dynamics of Air Combat," *Journal of Aircraft*, Vol. 20, July 1983, pp. 594-598.

[2]Herbst, W. B., "Supermaneuverability," *Unsteady Separated Flows*, edited by M. S. Francis and M. W. Luttges, University Colorado Press, Boulder, 1983, pp. 1-9.

[3]McCroskey, W. J., Carr, L. W., and McAlister, K. W., "Dynamic Stall Experiments on Oscillating Airfoils," *AIAA Journal*, Vol. 14, Jan. 1976, pp. 57-63.

[4]McCroskey, W. J., "Unsteady Airfoils," *Annual Review of Fluid Mechanics*, Vol. 14, Jan. 1982, pp. 285-311.

[5]McCroskey, W. J. and Pucci, S. L., "Viscous-Inviscid Interaction on Oscillating Airfoils in Subsonic Flow," *AIAA Journal*, Vol. 20, Feb. 1982, pp. 167-174.

[6]Robinson, M. C. and Luttges, M. W., "Unsteady Flow Separation and Attachment Induced by Pitching Airfoils," AIAA Paper 83-0131, 1983.

[7]Walker, J. M. and Helin, H. E., "An Experimental Investigation of an Airfoil Undergoing Large Amplitude Pitching Motions," AIAA Paper 85-0039, 1985.

[8]Helin, H. E. and Walker, J. M., "Interrelated Effects of Pitch Rate and Pivot on Airfoil Dynamic Stall," AIAA Paper 85-0130, 1985.

[9]Baldwin, B. S. and Lomax, H., "Thin Layer Approximation and Algebraic Model for Separated Turbulent Flows," AIAA Paper 78-257, 1978.

[10]Cheng, H. K., "Lifting-Line Theory for Oblique Wings," *AIAA Journal*, Vol. 16, Nov. 1978, pp. 1211-1213.

[11]Hoeijmakers, H. W. M., Vaatstra, W., and Verhaagen, N. G., "On the Vortex Flow over Delta and Double-Delta Wings," AIAA Paper 82-0949, 1982.

[12]Gad-el-Hak, M. and Blackwelder, R. F., "The Discrete Vortices from a Delta Wing," *AIAA Journal*, Vol. 23, June 1985, pp. 961-962.

[13]Legendre, R., "Ecoulement au Voisinage de la Pointe Avant D'une Aile a Forte Fleche aux Incidences Moyennes," *La Recherche Aeronautique*, Vol. 30, 1952, pp. 3-8.

[14]Brown, C. E. and Michael, W. H., "Effect of Leading-Edge Separation on the Lift of a Delta Wing," *Journal of the Aeronautical Sciences*, Vol. 21, 1954, pp. 690-694.

[15]Smith, J. H. B., "Improved Calculations of Leading-Edge Separation from Slender, Thin, Delta Wings," *Proceedings of the Royal Society of London*, Ser. A, Vol. 306, 1968, pp. 69-90.

[16]Nayfeh, A. H., Mook, D. T., and Yen, A., "The Aerodynamics of Small Harmonic Oscillations Around Large Angles of Attack," AIAA Paper 79-1520, 1979.

[17]Konstadinopoulos, P., Mook, D. T., and Nayfeh, A. H., "A Numerical Method for General Unsteady Aerodynamics," AIAA Paper 81-1877, 1981.

[18]Konstadinopoulos, P., Mook, D. T. and Nayfeh, A. H., "Numerical Simulation of the Subsonic Wing-Rock Phenomenon," AIAA Paper 83-2115, 1983.

[19]Adler, J. N., Robinson, M. C., Luttges, M. W., and Kennedy, D. A., "Visualizing Unsteady Separated Flows," *Flow Visualization*, Vol. 3, edited by W. J. Yang, Hemisphere Publishing Corp., New York, 1985, pp. 342-347.

[20]Adler, J. N. and Luttges, M. W., "Three-Dimensionality in Unsteady Flow About a Wing," AIAA Paper 85-0132, 1985.

[21]Gad-el-Hak, M., Blackwelder, R. F., and Riley, J. J., "On the Growth of Turbulent Regions in Laminar Boundary Layers," *Journal of Fluid Mechanics*, Vol. 110, Sept. 1981, pp. 73-95.

[22]Gad-el-Hak, M., "The Use of the Dye-Layer Technique for Unsteady flow Visualization," *Journal of Fluids Engineering*, Vol. 108, March 1986, pp. 34-38.

[23]Didden, N. and Ho, C.-M., "Unsteady Separation in the Boundary Layer Produced by an Impinging Jet," *Journal of Fluid Mechanics*, Vol 160, Nov. 1985, pp. 235-256.

[24]Ho, C.-M., "An Alternative Look at the Unsteady Separation Phenomenon," *Recent Advances in Aerodynamics*, edited by A. Krothapalli and C. A. Smith, Springer-Verlag, New York, 1986, pp. 165-178.

[25]Gad-el-Hak, M. and Ho, C.-M., "Three-Dimensional Effects on a Pitching Lifting Surface," AIAA Paper 85-0041, 1985.

[26]Gad-el-Hak, M., Ho, C.-M., and Blackwelder, R. F., "A Visual Study of a Delta Wing in Steady and Unsteady Motion," *Unsteady Separated Flows*, edited by M. S. Francis and M. W. Luttges, University of Colorado Press, Boulder, 1983, pp. 45-51.

[27]Gad-el-Hak, M., and Ho, C.-M., "The Pitching Delta Wing," *AIAA Journal*, Vol. 23, Nov. 1985, pp. 1660-1665.

[28]Winkelmann, A. E. and Barlow, J. B., "Flowfield Model for a Rectangular Planform Wing beyond Stall," *AIAA Journal*, Vol. 18, Aug. 1980, pp. 1006-1008.